Received: 27 February 2023 | Revised: 25 May 2023 | Accepted: 9 June 2023

DOI: 10.1111/jace.19305

Journal of the American Ceramic Society

RESEARCH ARTICLE

Ceramics with eutectic microstructure in the ZrO_2–PrO_x system

Lorena Grima | **José Ignacio Peña** | **María Luisa Sanjuán**

Instituto de Nanociencia y Materiales de Aragón, Facultad de Ciencias, Universidad de Zaragoza-CSIC, Zaragoza, Spain

Correspondence
María L. Sanjuán, Instituto de Nanociencia y Materiales de Aragón (Universidad de Zaragoza-CSIC), Facultad de Ciencias, Universidad de Zaragoza, 50009 Zaragoza, Spain.
Email: sanjuan@unizar.es

Funding information
Spanish Government, Grant/Award Numbers: PID2019-107106RB-C32, PID2021-124863OB-I00, BES-2017-079683; European Union; The financial support from Gobierno de Aragón, Grant/Award Number: T02-20R group

Abstract

Praseodymium oxides present redox properties analogous to those of Ce-based systems and have been proposed for catalytic applications in combination with CeO_2, ZrO_2, or both. However, uncertainties remain concerning the nature and redox behavior of Pr-rich mixtures, especially with ZrO_2. Here we study the eutectic composites of the ZrO_2–PrO_x system, focusing on the sensitivity of their microstructure, phase symmetry, and composition to variations of the processing atmosphere from oxidizing to reducing. Mixed oxides have been produced by a laser-assisted directional solidification technique in O_2, air, N_2, or 5%H_2(Ar) environment, and the resulting materials have been analyzed by scanning electron microscopy/energy-dispersive X-ray spectroscopy, X-ray diffraction, Raman spectroscopy, and magnetic susceptibility. In air, N_2, or 5%H_2(Ar) atmosphere, a lamellar, eutectic-like microstructure forms, the major phase being the one with less Pr content. Both the Pr concentration in each phase as the PrO_x molar percentage of the eutectic composites decrease as the atmosphere becomes more reducing. Both eutectic phases are fluorite-like when processing in air, whereas in N_2 or 5%H_2(Ar), the phase with high Pr content is of the A-R_2O_3 type, and the phase with low Pr content can be described as a fluorite phase containing C-R_2O_3-like short-range-ordered regions. The results obtained for samples processed in O_2 suggest that for high enough pO_2 no eutectic forms, in analogy with the ZrO_2–CeO_2 system. The evolution of the phase composition and symmetry is discussed in terms of the limited stability of the phases found in the ZrO_2–Pr_2O_3 system, namely, A- or C-R_2O_3-like, beyond a certain Pr oxidation degree and oxygen content.

KEYWORDS
eutectic materials, laser processing, microstructure, oxidation, phase diagrams, praseodymium oxide, ZrO_2

1 | INTRODUCTION

Praseodymium oxides are receiving interest in recent times because of their redox properties, analogous to those of Ce-based systems, which make them promising for catalytic applications. Several studies have addressed the properties of PrO_x combined with CeO_2 and/or ZrO_2.[1–5] In the ZrO_2–PrO_x system, in particular, higher reducibility and lower temperatures of reduction are obtained for Pr-rich compositions (Pr/Zr > 1).[2,4,5] Despite the technological interest, the high Pr content/high-temperature region of the phase diagram is still quite uncertain, an aspect that may be related to the mixed-valence properties of Pr.[6–8] According to the early studies in the 70′s and 80′s, all ZrO_2–R_2O_3 systems (R = La to Yb) present a eutectic point in the R-rich side of the phase diagram at a molar proportion of R_2O_3 between 65 and 85 mol%.[7–9] For the ZrO_2–Pr_2O_3 system, the eutectic is found at 70 mol% Pr_2O_3 and is composed of a low Pr content phase of bixbyite C-R_2O_3 type ($Ia\bar{3}$ space group [SG]), with 62 mol% Pr_2O_3, and a high Pr content cubic phase, labeled as X phase, with 78 mol% Pr_2O_3, which is stable only near the melting point.[7] Converting molar percentages from Pr_2O_3 to $PrO_{1.5}$, the eutectic would be at 82.4 mol% $PrO_{1.5}$, with low and high Pr content phases at 76.5 and 87.6 mol% $PrO_{1.5}$, respectively. The X phase was later analyzed (in the ZrO_2–La_2O_3 and ZrO_2–Nd_2O_3 systems) by neutron diffraction and found to have $Im\bar{3}m$ SG.[10] There exists, however, discrepancy among the two reported phase diagrams[6,7] (see Figure S1a,b). Among other differences, in Ref. [6], the low Pr content phase of the eutectic is said to be a "tetragonally deformed" fluorite. We note that the PD of Ref. [6] presents a lot of undefined regions; the details of the proposed phases, beyond their symmetry, are not given, neither the oxygen partial pressure in which data were collected. The text accompanying that PD in the PD database says that "the oxygen activity is not fixed experimentally."

In any case, in the ZrO_2–PrO_x system, the mixed-valence character of praseodymium anticipates a dependence of the eutectic characteristics on the oxygen partial pressure (pO_2) of the synthesis or processing atmosphere. In fact, in the closely related ZrO_2–CeO_x system, where Ce also presents mixed-valence properties, a eutectic point exists for total Ce reduction (at ~87 mol% $CeO_{1.5}$[11]) but not in the oxidized ZrO_2–CeO_2 system.[12] In Ref. [7], Rouanet studied the effect of quenching ZrO_2–PrO_x mixtures from the melt to room temperature (RT) in air, but eutectic properties such as phase composition and lattice parameters were not analyzed. Moreover, eutectic microstructures were not described either in reducing or in oxidizing conditions. In this work, we analyze the composition, symmetry, and dependence on the processing atmosphere of the ZrO_2–PrO_x eutectic composites.

Mixed oxides have been produced by the laser-assisted directional solidification technique, also known as laser-floating zone (LFZ), which allows reaching the high melting point of these oxides and controlling the growth atmosphere during melting and cooling. The resulting materials have been characterized by scanning electron microscopy (SEM) and energy-dispersive X-ray spectroscopy (EDX) to determine the phase composition and ZrO_2–PrO_x proportion as a function of the processing atmosphere (O_2, air, N_2, or 5%H_2(Ar)), and by X-ray diffraction (XRD) and Raman spectroscopy to identify the phase symmetry. Magnetic susceptibility has been used to investigate the oxidation state of one of the samples. We find good agreement with early works for samples produced in 5%H_2(Ar) but different phases are found in oxidizing atmosphere, as expected.

The main idea behind this work is that advancing in the knowledge of the chemical and structural properties of Pr-rich ZrO_2–PrO_x composites in environmental conditions varying from reducing to oxidizing may help in the design of catalysts based on mixed-valence elements, particularly in those containing Pr.

2 | EXPERIMENTAL METHODS

Ceramic rods of $Zr_{1-x}Pr_xO_y$ with different Pr content were prepared by solid-state reaction. Powders of Pr_6O_{11} (99.9%, Merck) and ZrO_2 (99%, Merck) previously heated at 1200°C were mixed in the adequate proportion so as to get the desired nominal compositions. Rodlike precursors were isostatically pressed at 200 MPa and then sintered at 1500°C in air during 12 h. The sintered rods presented a diameter between 3 and 4 mm and were roughly 7 cm in length. Crystalline samples with a diameter of approximately 2 mm were grown, from the sintered rods, by the LFZ technique using a CO_2 laser ($\lambda = 10.6\ \mu$m) as a heating source (Blade-600, Electronic Engineering) at a growth rate of 300 or 100 mm/h. To study the influence of the processing atmosphere on the eutectic microstructure and phase composition, samples were grown in different atmospheres (O_2, air, N_2, and 5%H_2 in Ar), thus varying the conditions from oxidizing to reducing. The growth chamber was kept at a slight overpressure of 0.1–0.25 bar with respect to ambient pressure.

Compositional analysis and morphology were characterized by field emission SEM (FESEM) using a Carl Zeiss MERLIN microscope with an EDX detector incorporated.

X-ray diffraction patterns were collected with a D-Max Rigaku, RU300 diffractometer, using the Cu K_α radiation.

TABLE 1 Pr contents (PrO_x mol%) derived from energy-dispersive X-ray spectroscopy (EDX) analyses, lattice parameters (Å), and unit cell volume per $Zr_{1-x}Pr_xO_y$ formula (V_f, in $Å^3$) of phases forming the eutectic-like composites of the ZrO_2–PrO_x system processed in different atmospheres.

Processing atmosphere	Average PrO_x mol%	Light (high-Pr) phase			Dark (low-Pr) phase			% vol. dark phase	Δ PrO_x mol%
		PrO_x mol%	Latt. param.	V_f	PrO_x mol%	Latt. param.	V_f		
O_2, oxidized ring	87.15	93.3	$a_F = 5.432$ ($Pr^{3.87+}$, $O_{1.94}$)	80.1	86.6	$a_F = 5.421$ ($Pr^{3.84+}$, $O_{1.93}$)	79.6	>90	6.7
O_2, reduced core	86.5	92.6	$a_F = 5.478$ ($Pr^{3.74+}$, $O_{1.88}$) $a_A = 3.838$, $c_A = 6.072$	82.2 77.5	84.2	$a_F = 5.460$ ($Pr^{3.69+}$, $O_{1.87}$)	81.4	73–82	8.4
Air	85.9	91.7	$a_F = 5.440$ ($Pr^{3.84+}$, $O_{1.93}$)	80.5	83.3	$a_F = 5.427$ ($Pr^{3.78+}$, $O_{1.91}$)	79.9	70	8.4
N_2	82.2	88.3	$a_A = 3.837$, $c_A = 6.071$	77.4	76.2	$a_C = 10.909$	81.1	61	12.1
5%H_2(Ar)	82.3	87.3	$a_A = 3.835$, $c_A = 6.071$	77.3	76.4	$a_C = 10.902$ ($Pr^{3.07+}$, $O_{1.64}$)	81.0	47.4	10.9

Note: F, A, and C subindices stand for fluorite-, A-R2O3-, and C-R2O3-like phases, respectively. The Pr oxidation states derived either from the relation between the lattice parameter and ionic radii (in fluorite phases) or from the magnetic susceptibility (in the C-phase of the eutectic processed in 5%H2(Ar)) are given in brackets, as well as the resulting O stoichiometry). The relative volume of the dark (low-Pr) phase and the compositional separation between the high- and low-Pr phases (Δ) are also given.

Abbreviation: Latt. param., Lattice parameter.

Patterns were measured from 5° to 80° with $\Delta 2\theta = 0.03°$ and 1 or 3 s/step. Lattice parameters were determined with the help of the FullProf software.[13]

Raman measurements were performed using a DILOR XY spectrometer equipped with a liquid nitrogen–cooled CCD detector. Spectra were taken at RT with a ×50 microscope objective lens, using the 514.5 or 496.5 nm lines of an Ar^+ laser (model Coherent INNOVA 305).

Magnetic susceptibility was derived from magnetization measurements, under a magnetic field of 1000 Oe, performed on a SQUID detector magnetometer Quantum Design MPMS5.

3 | EXPERIMENTAL RESULTS

3.1 | Sample growth

Ceramic rods of mixed ZrO_2–PrO_x oxides were processed following the procedure described above. The PrO_x content of the mixtures was varied around 85% until eutectic microstructures were found. The compositions yielding eutectic microstructures in the four atmospheres used are listed in Table 1. The sample color varied from dark green (in reducing atmosphere) to almost black (in oxidizing atmosphere), indicating differences in the Pr oxidation state (see Figure S2). Transverse sections were cut and polished for electron microscopy and Raman experiments.

3.2 | Electron microscopy

The sample microstructure and elemental composition were analyzed by SEM and EDX, respectively. Figure 1A–D shows images of the transverse sections of samples processed in O_2, air, N_2, and 5%H_2(Ar) at either 300 or 100 mm/h. Eutectic-like lamellar microstructures are found in all four atmospheres, consisting of alternating dark-contrast (low Pr content) and light-contrast (high Pr content) phases, although in samples processed in O_2 at 300 mm/h only a central region of the processed rod displayed this eutectic-like aspect. For short, the low and high Pr content phases will be just called low-Pr and high-Pr phases, respectively. The lamellae interspacing is between 1.5 and 2.5 μm, and imperfect alignment is attributed to the high solidification rates used to prevent Pr volatilization. All parameters describing the lamellar microstructure and chemical composition vary with the processing atmosphere, as collected in Table 1. As the atmosphere evolves from more oxidizing (O_2) to more reducing (5%H_2(Ar)), the following trends are observed: (i) The volume proportion of the dark phase decreases from ~78% to ~50%. (ii) The Pr content of both phases decreases, from 84.2 to 76.4 PrO_x mol% for the dark phase and from 92.6 to 87.3 PrO_x mol% for the light phase, implying that the compositional difference between high- and low-Pr phases (Δ) increases from ~8 to ~11 mol% PrO_x. (iii) The simultaneous variation of the phase composition and of the phase proportion with the atmosphere results in a much smoother variation of the average composition, from 87 to 82 mol% PrO_x.

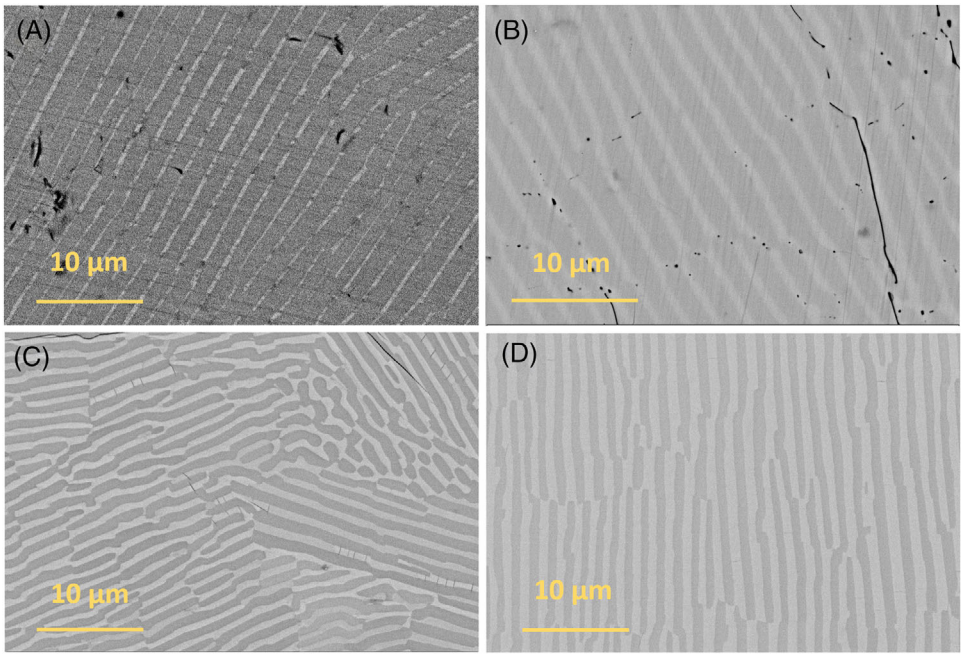

FIGURE 1 Transverse section images of ZrO_2–PrO_x samples solidified by laser-floating zone (LFZ) in (A) O_2, (B) air, (C) N_2, and (D) 5%H_2(Ar) atmospheres. Sample (B) was processed at 100 mm/h, all the others at 300 mm/h. Part (A) belongs to the central part of the rod processed in O_2.

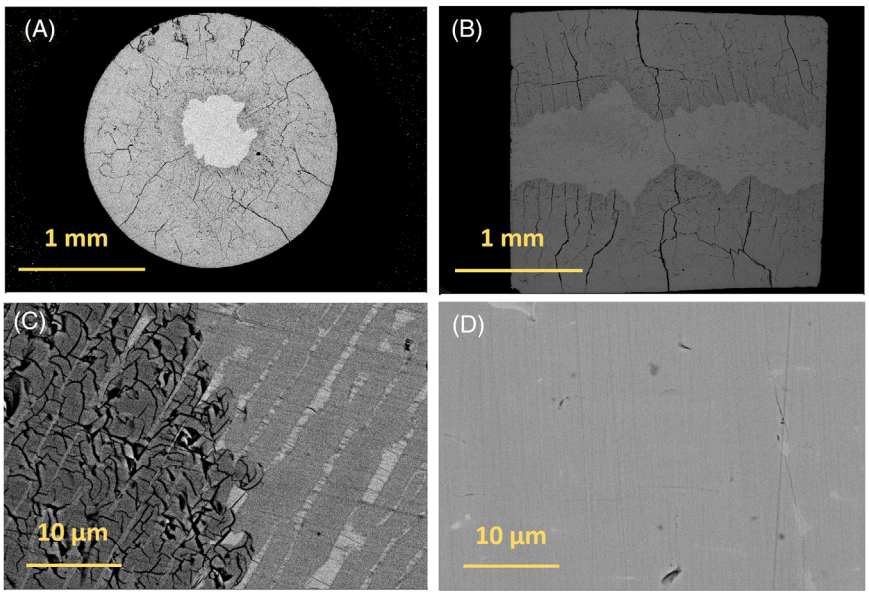

FIGURE 2 Transverse (A) and longitudinal (B) sections of the sample processed in O_2 at 300 mm/h, displaying separation between a light-contrast (reduced) inner core and a dark-contrast (oxidized) outer ring. Part (C) shows the border between the inner and outer regions of the same sample. Part (D) displays a section of a sample with the same average composition as that in parts (A–C) processed in O_2 at 100 mm/h, to highlight the disappearance of a eutectic microstructure.

The phase compositions (76.4 and 87.3 mol% PrO_x for the low and high-Pr phases, respectively) of the eutectic processed in 5%H_2(Ar) are similar to those found at high temperatures in Ref. [7] also in reducing conditions (76.5 and 87.6 mol% $PrO_{1.5}$, respectively).

It has to be noted that the sample processed in O_2 at 300 mm/h presented a core–shell aspect (Figure 2A,B) with a light-contrast core surrounded by a dark-contrast outer ring. A magnification of the border between both regions (Figure 2C) evidenced the presence of many cracks in the outer ring, suggesting the occurrence of thermo-mechanical stresses during solidification. Figure 2 also shows that the lamellar microstructure seems to faint in the outer region, to the point that any phase separation is hard to distinguish (Figure 1A belongs to the central region). EDX analyses showed that the central core had a slightly lower average Pr content than the outer region. The Pr content of each phase forming the composite was also different, as collected in Table 1. The core–shell aspect is attributed to incomplete oxygen uptake, resulting in an

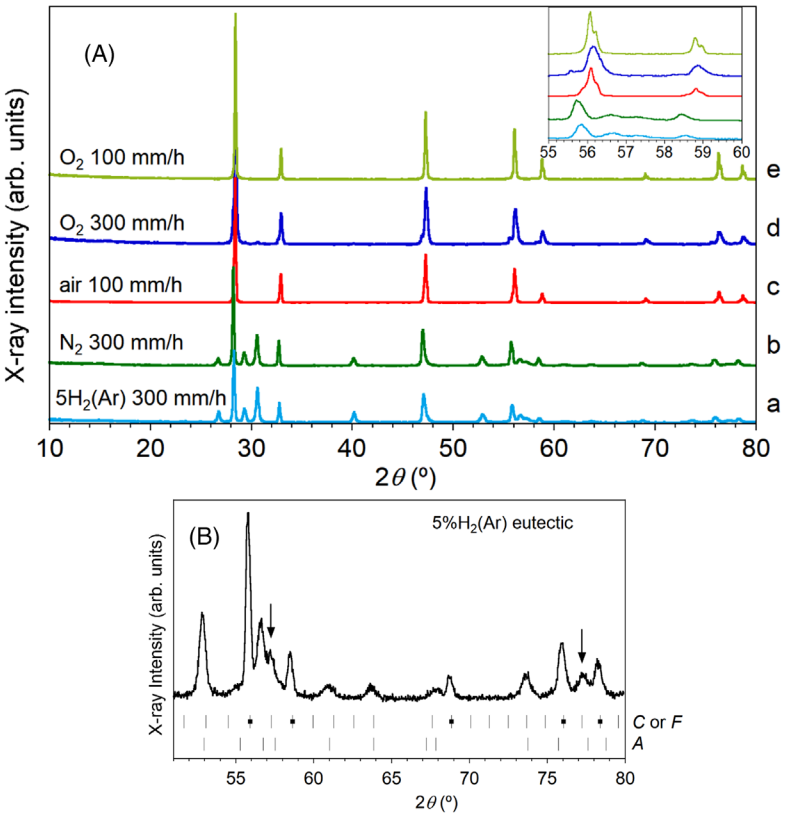

FIGURE 3 (A) X-ray diffraction (XRD) patterns of ZrO_2–PrO_x eutectics processed in 5%H_2(Ar) (A), N_2 (B), air (C), and O_2 (D), at the indicated rates. Pattern (E) belongs to a sample processed in O_2 at 100 mm/h, not displaying a eutectic microstructure (see Figure 2D). The inset shows a magnification of the 55°–60° region to highlight the presence of more than one phase in all cases except for the sample processed in O_2 at 100 mm/h, which evidences a single fluorite pattern. (B) The 50°–80° region of the pattern of the eutectic processed in 5%H_2(Ar) is magnified, to highlight the regions where the fit requires cell-doubling (marked with arrows). Tics marked with a square denote the fluorite-substructure reflections, which are common to C and F phases.

oxidized outer region surrounding a more reduced core. The above observations lead us to conclude that the outer region has lost the eutectic character. In fact, also the aspect of the inner core is anomalous, compared with proper eutectic composites obtained in air, N_2, or 5%H_2(Ar) (Figure 1B–D). The volume proportion of the dark phase, for instance, is quite below the limit (29%) that usually implies a change from lamellar to fibrilar–like eutectic microstructure.[14]

The preceding results suggest that no eutectic would form in the totally oxidized case. To verify this hypothesis, a sample with the same average Pr content was processed at a lower rate of 100 mm/h. As Figure 2D shows, the slowly processed sample displays a homogenous microstructure with no eutectic separation. We interpret that the slow growth enables oxygen diffusion throughout the whole sample so as to reach a homogeneous, single-oxidized phase. We will comment on these facts in Section 4.

3.3 | X-ray diffraction

The XRD patterns of ZrO_2–PrO_x eutectic or quasi-eutectic samples processed in 5%H_2(Ar), N_2, air, and O_2 are shown in Figure 3A (patterns a–d, respectively). Phase content and lattice parameters were analyzed with the help of the FullProf software.[13] The lattice parameters obtained from the profile fits are collected in Table 1. Although the most intense peaks are characteristic of a fluorite-like phase, an accurate fit requires at least a second minor phase. For comparison, we show in Figure 3A-E the pattern of the sample processed in O_2 at 100 mm/h, which can be explained by a single fluorite phase, with $a = 5.4334$ Å. A clear difference exists between eutectic samples processed in oxidizing atmospheres (see Figure S3), where both phases are of the fluorite (F) type (SG $Fm\bar{3}m$), and those processed in neutral or reducing atmospheres (Figure S4), where the main phase is fluorite-like and the minor phase is a trigonal phase of the A-R_2O_3 type (SG $P\bar{3}m_1$).

Looking in more detail at the diffraction patterns of the eutectics processed in N_2 and 5%H_2(Ar), we find peaks (specifically at ~57.2° and 77.2°, see Figure 3B) that are not explained by either the fluorite or the A phase of the F + A model. The phase attribution made in Ref. [7], where C + A phases were found in a reducing atmosphere, and the similarity between the chemical compositions of the eutectic phases reported in Ref. [7] with those of our eutectic processed in 5%H_2(Ar) led us to suspect that the low-Pr phase of the samples processed in N_2 or 5%H_2(Ar) might be a bixbyite phase instead of a fluorite one. In fact, the peaks around 57.2° and 77.2° are nicely explained as the (3 6 1) and (7 5 2) peaks, respectively, of a C-like phase with $Ia\bar{3}$ SG and $a_C \approx 2a_F$.

Although the C + A model clearly improves the F + A fit (see Figures S4b,d), an intriguing question arises as to why

the low angle superstructure peaks related to cell doubling, in particular the (211) peak at ~20°, are not observed in patterns (a) and (b) of Figure 3. An intense peak at that angle, for instance, was found in Ref. [5] for a 98 mol% PrO_x-rich sample, initially with F structure, which transformed to C-phase after a 15 h reducing treatment at 900°C. We speculate that the absence of clear superstructure peaks at low angle may be related to the disordered character of the C-like phases found in our samples. Disorder occurs both in the cation sublattice, because of the presence of ~24% Zr^{4+} cations per formula unit (pfu), as in the oxygen sublattice, with oxygen excess coming from charge compensation for Zr^{4+} as well as for some degree of Pr oxidation. Disordered fluorites are prone to order–disorder phenomena such as domain formation with short-range ordering at a few unit cell scale, resulting in the appearance of superstructure peaks related to the ordered regions. This is typically observed in systems undergoing order–disorder phase transitions with cell-doubling, such as the F to pyrochlore or F-to-C transitions. Depending on the domain size, peak broadening may affect to a greater degree the superstructure peaks and, from those, the low-angle ones, as in our case.[15] Thus, the low-Pr phase of the eutectic processed in 5%H_2(Ar) may be described as a fluorite phase containing vacancy-ordered C–like regions. The C + A model is further supported by Raman scattering results (section 3.4), where bands attributable to C and A-like phases are observed, and by arguments based on the relation between the stability of fluorite-like lattices and the concentration of anionic vacancies, as discussed in Section 4.

The case of the sample processed in O_2 is particular, because its pattern cannot be explained with only two phases. Both the detection of weak additional peaks as the asymmetric shape of the main reflections suggest the presence of at least four phases: two very close fluorite phases with $a_1 \sim 5.42$ Å and $a_2 \sim 5.43$ Å for the intense reflections, and another pair of fluorite phases with larger parameters, $a_3 \sim 5.46$ Å and $a_4 \sim 5.48$ Å, for the minor reflections at the low angle side of the most intense ones. A low amount of trigonal A-R_2O_3-like phase is also required to explain the weak reflections at 29.4°, 30.7°, and 40.2°, detectable only at high magnification scale. The explanation for the presence of four fluorite-like phases is clear when we see the images of the transverse and longitudinal sections of that sample (Figure 2). We have attributed the core–shell aspect to incomplete oxygen uptake. At the high melting temperatures, Pr ions would be highly reduced, even in O_2; upon cooling and solidification, oxygen uptake progresses radially but, because of the fast cooling rates, diffusion becomes progressively slower and does not reach the rod center. Thus, the final state of the sample consists of a reduced center and a more oxidized outer region. The

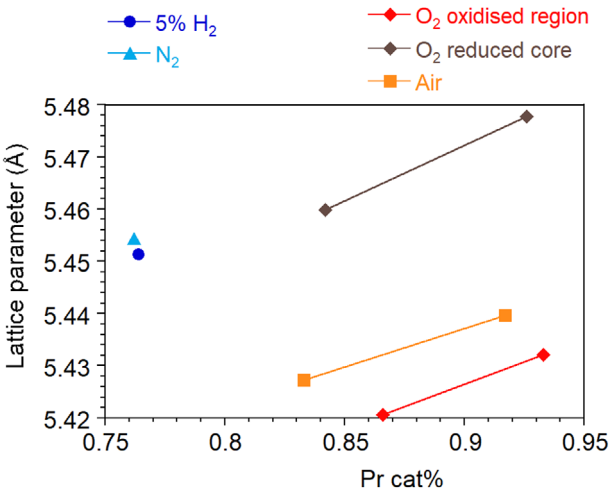

FIGURE 4 Lattice parameters of the fluorite-type phases found in the eutectic-like composites of the ZrO_2–PrO_x system processed in different atmospheres, as a function of the Pr cation content. The lattice parameters of C-R_2O_3 phases have been divided by two to normalize to the fluorite unit cell.

cracks in the outer region are attributed to the contraction produced upon oxidation. According to Figure 2, the volume proportion of the reduced core is ≲10%.

The two fluorite-like phases with smaller lattice parameters (a_1, a_2) are assigned to the oxidized ring whereas the two fluorite phases with larger lattice parameters (a_3, a_4) and low intensity are assigned to the partially reduced eutectic-like core. The appearance of a weak amount of A-like phase is attributed to the incomplete transformation of the high-Pr phase of the reduced region to a fluorite phase. Note that the lattice parameters of the reduced-core phases are considerably larger than those of the oxidized ring, despite the Pr contents being close, which is attributed to the larger ionic radius of Pr^{3+} compared to Pr^{4+}. With this assignment, the relation between chemical composition and lattice parameters is as shown in Figure 4. Two trends of increasing lattice parameters are observed: the first one goes from left to right and is due to increasing Pr content, as expected. The second one goes from bottom to top and is related to increasing reduction for fixed Pr content.

Some X-ray measurements were repeated several months after the first data collection. They evidenced the presence of $Pr(OH)_3$ in samples containing A-like phases but not in samples where the Pr-rich phase was fluorite-like. We attribute the presence of $Pr(OH)_3$ to the hydration of A-Pr_2O_3, which is known to react with ambient humidity.[16]

The diffraction results can be further exploited to get information about the Pr oxidation state in fluorite-like phases, taking benefit of the relation $R_C + R_O = a\sqrt{3}/4$ between the lattice parameter (a) and the ionic radii of its constituting elements, R_C and R_O being the

cation and oxygen ionic radii in eight- and fourfold coordination,[17] respectively. Using the lattice parameters collected in Table 1 and R_O = 1.38 Å, we derive the average cation radius of each phase, R_C, and write it as $R_C = \alpha R_{Pr} + (1-\alpha)R_{Zr}$, α being determined by EDX analyses. Taking R_{Zr} = 0.84 Å,[17] we extract the effective Pr radius, R_{Pr}, which is, in turn, an average over Pr^{3+} and Pr^{4+} radii, $R_{Pr} = \beta R_{Pr3+} + (1-\beta)R_{Pr4+}$, with R_{Pr3+} = 1.126 Å and R_{Pr4+} = 0.96 Å.[17] This yields the relative Pr^{3+}/Pr^{4+} content. XRD is advantageous in that the patterns of all phases present in the sample are superposed but not averaged, so that the oxidation states of the low and high Pr phases can be obtained separately. Applying this procedure to the fluorite-like phases found in samples processed in air or O_2, we find Pr oxidation states ranging from $Pr^{3.7+}$ to $Pr^{3.9+}$. The values obtained are collected in Table 1.

We note that the expression $R_C + R_O = a\sqrt{3}/4$ assumes eightfold cation coordination, whereas the average cation coordination would be smaller than eight in a defective fluorite. However, we have considered that in samples processed under oxidizing atmospheres, the vacancy concentration would be low and assumed the expression to be valid, at least in a qualitative way. The high oxidation states obtained support our assumption. For C-like phases, where the cation coordination is sixfold, the relation is no longer valid and cannot be used to derive the Pr oxidation state. Magnetic measurements are performed instead (see Section 3.5).

3.4 | Raman spectroscopy

Raman spectroscopy was used to support the phase assignment. With its short coherence length, this technique is ideally suited to detect short-range ordering effects as those expected in our materials.[18] Figure 5 shows representative spectra of samples processed in O_2 and 5%H_2(Ar). The sample processed in 5%H_2(Ar) presents narrow peaks at 108, 190, and 416 cm^{-1}, very close to those of A-Pr_2O_3,[19] which we assign to the Pr-rich component of the eutectic. Three more peaks at 143, 295, and 356 cm^{-1} arise from $Pr(OH)_3$ developed upon exposure to air.[20,21] The identification of $Pr(OH)_3$ is supported by the detection of the OH^- stretching band at 3605 cm^{-1}. The narrow peaks are superposed to broad bands centered around 340, 580, 670, and 800 cm^{-1}, assigned to the low-Pr phase with perhaps some admixture of Pr^{3+} crystal-field transitions.

To clarify the band assignment, we processed in 5%H_2(Ar) a sample of $Pr_{0.75}Zr_{0.25}O_x$ stoichiometry, close to that of the low-Pr phase of the eutectic processed in 5%H_2(Ar). Its spectrum (Figure 5) presents a broad intense band centered at 330 cm^{-1} and a weaker one at 660 cm^{-1},

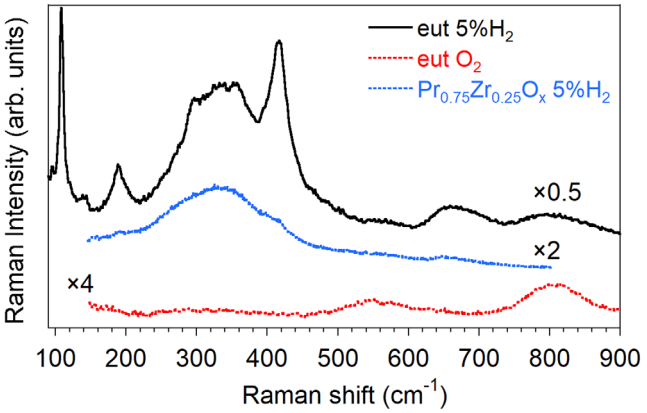

FIGURE 5 The Raman spectra of the ZrO_2–PrO_x eutectic composite processed in 5%H_2(Ar) (top spectrum, in black) is compared with that of the sample processed in O_2 (bottom spectrum, in red) and with that of the $Pr_{0.75}Zr_{0.25}O_x$ compound processed in 5%H_2(Ar) (in blue).

thus supporting the attribution of these two bands to the low-Pr phase. It is interesting that the wavenumber of the main band is similar to that of the related C-R_2O_3 compounds (312 cm^{-1} for metastable C-La_2O_3,[22] and 335 cm^{-1} for metastable C-Nd_2O_3[23]).

The broad aspect of the bands assigned to the low-Pr phase is not surprising, owing to the presence of cation chemical disorder and partially-filled anion vacancies. The spectrum, however, supports our attribution of the low-Pr phase to a bixbyite phase and not to a fluorite one. In fluorite-like stabilized cubic zirconia (YSZ), for instance, the Raman spectrum resembles more a density of states than the single mode expected for a well-ordered fluorite and extends up to 600 cm^{-1}, although in nanometric c-ZrO_2, a single broad band ascribed to the fluorite T_{2g} mode is found at 490 cm^{-1}.[24] On the other hand, the main band in PrO_2 appears at 430 cm^{-1} and is also attributed to the fluorite T_{2g} mode.[25] In our case, the spectrum of the low-Pr phase found in reducing atmosphere differs considerably both from the density-of-states-aspect of stabilized zirconia but also from that of well-ordered fluorites and, as we have seen, agrees with the trend expected for a C-type phase. In samples processed in O_2 or in air, the spectrum is even more featureless because both phases are disordered fluorites.

3.5 | Magnetic susceptibility

The oxidation state of the low-Pr phase of the eutectic processed in 5%H_2(Ar) was derived from magnetic susceptibility measurements (Figure 6). The data analysis in eutectic systems is hindered by the presence of two magnetic phases with different compositions where, moreover,

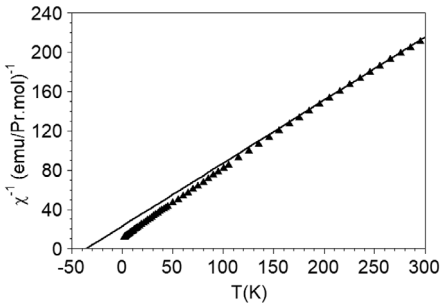

FIGURE 6 Inverse magnetic susceptibility per Pr ion of the low Pr phase of the eutectic processed in 5%H_2(Ar). The data have been derived from the total susceptibility, which includes the contributions of the low and high Pr phases, by the procedure outlined in the text. Triangles are the experimental points, and the line is the fit to a Curie–Weiss law in the 195–295 K range.

the Pr oxidation state may differ. To extract the Pr oxidation state, we have proceeded as follows:

We assume that the sample is composed of two phases L and H, with low and high Pr contents, and molar contents n_L and n_H, respectively. We also assume that the Pr content pfu of each phase is given by $[Pr]_L$ and $[Pr]_H$, respectively. Knowing the sample mass and average composition, both $n_{L,H}$ and $[Pr]_{L,H}$ are determined from an EDX analysis of each phase and of the average sample (see Table 1).

The total magnetic susceptibility $\chi = \chi_L + \chi_H$ can be written in terms of the molar and Pr content of each phase as $\chi = n_L[Pr]_L\chi_{mL} + n_H[Pr]_H\chi_{mH}$, where $\chi_{mL} = \chi_L/n_L[Pr]_L$ and $\chi_{mH} = \chi_H/n_H[Pr]_H$ are the susceptibilities per Pr ion in the L and H phases, respectively. To separate the contribution of both phases, we assume that the Pr-rich A-like phase is completely reduced. The assumption is justified by the small tolerance of the A phase to cation oxidation. Assuming for the H phase a Curie–Weiss (CW) dependence in the 200–300 K range, χ_{mH} is written as $\chi_{mH} = [C/(T - \theta)]$, where the Curie constant C fulfills $8C = \mu_{eff}{}^2$, and we take $\mu_{eff,H} = \mu(Pr^{3+}) = 3.58\ \mu_B$ and $\theta = -73$ K, the value reported for A-Pr_2O_3.[26]

Then, we subtract $\chi_H = n_H[Pr]_H\chi_{mH}$ from the total susceptibility, to get χ_L. Knowing n_L and $[Pr]_L$ from EDX, we work out χ_{mL} and fit it to another CW law at high temperature, which gives $\mu_{eff,L} = 3.52\ \mu_B$. Finally, writing $\mu_{eff,L}{}^2 = \varepsilon\mu_{Pr3+}{}^2 + (1 - \varepsilon)\ \mu_{Pr4+}{}^2$ and taking the reference values $\mu_{Pr3+} = 3.58\mu_B$ and $\mu_{Pr4+} = 2.54\mu_B$ for Pr^{3+} and Pr^{4+} in their ground-state multiplets, respectively, we find $\varepsilon = 0.93$, that is, a very low oxidation state $Pr^{3.07+}$ for Pr ions in the low-Pr phase of the 5%H_2(Ar) eutectic. The result is in agreement with the greenish color of the sample (Figure S2).

4 | DISCUSSION

The preceding results evidence that eutectic-like lamellar microstructures are formed in directionally solidified ZrO_2–PrO_x mixed oxides at compositions around 82–87 mol% PrO_x when the processing atmosphere is either reducing (5%H_2(Ar)), neutral (N_2) or partially oxidizing (air). However, the sample processed in O_2 behaves in a clearly different way and provides a hint of the system behavior under extremely oxidizing conditions. The two-region aspect of that sample, with a reduced inner core surrounded by an oxidized outer ring, suggests incomplete oxidation during cooling. Both the microstructure and the elemental analysis indicate that no eutectic is produced in the outer region and, if at all, in an anomalous way in the inner core. The homogeneous microstructure of a sample with the same average Pr content, processed in O_2 at a lower rate of 100 mm/h, and the single-fluorite character of its XRD pattern, confirm that no eutectic exists in the limit of total oxidation.

The evolution of the eutectic composition and phase symmetry in the ZrO_2–PrO_x system upon changing the processing atmosphere, as well as the likely absence of a eutectic point in the O_2 case, can be understood in relation with the trend observed in the eutectics of the ZrO_2–R_2O_3 series and would be, as most structural properties of rare-earth compounds, dictated by the relation between phase stability, average cation size, and vacancy concentration.[7,9] According to Ref. [7], the average rare-earth content in the eutectic increases as the rare-earth size decreases, from 62.5 mol% R_2O_3 for R = La to 82 mol% for R = Ho, Er, and Y. The composition of the high-R phase, in turn, increases from 70 to 95 mol% of R_2O_3 along the series. This evolution can be attributed to the limited stability of the A-R_2O_3 structure: As the rare-earth size decreases, the stable phase of the R_2O_3 compounds evolves from A-type first to B (a monoclinic structure closely related to A-phase) and then to C-type.[27] The increasing rare-earth content at the high-R phase warrants the eutectic occurrence as a C + A or C + C′ combination of phases, depending on the effective ionic radii. As regards the low-R phase, with R content increasing from 55 to 70 mol% R_2O_3 along the series, its C-like structure can be ascribed to the higher tolerance of the bixbyite lattice to anion vacancies, compared with the fluorite one, and to small cations like Zr^{4+}, compared with the A-phase.

The same ideas can be applied to the ZrO_2–PrO_x system upon changing the processing atmosphere or the temperature, allowing for the effective cation size dependence on both the (Pr, Zr) stoichiometry as on the Pr oxidation state. First, we note that the ionic radius of Pr^{4+} in eightfold coordination is 0.96 Å, just slightly smaller than Yb^{3+} in

the same coordination (0.985 Å),[17] for which the occurrence of a eutectic point is doubtful.[7] This suggests that the fully oxidized Pr^{4+} ion is too small to form a eutectic, which supports our proposal that the microstructure of the sample processed in O^2 should be rather ascribed to phase evolution upon cooling (see below). For less severe oxidation, the symmetry and composition of the eutectic phases will depend mainly on the effective ionic radius in the high-Pr phase, allowing for the decrease of the Pr size from 1.126 Å for Pr^{3+} to 0.96 Å for Pr^{4+}.[17] In analogy with the eutectics of the ZrO_2–R_2O_3 series, combinations going from C + A to C + C phases might be expected for increasing oxidation degree if only the variation of the ionic radii were considered. The ZrO_2–PrO_x system has, however, the added ingredient of increasing oxygen content to compensate for higher Pr oxidation states, so that in the presence of high enough O_2 concentration, C phases are expected to evolve toward F phases and A phases into C or F phases. This explains, in general terms, the C + A phases obtained in N_2 and 5%H_2(Ar) atmospheres, and the F + F phases found in air.

The relation among Pr oxidation state, vacancy content, and the formation of F-, C-, or A-like phases is clearly exemplified in our eutectics. In preceding sections, we have shown that two ranges of oxidation states are found: between $Pr^{3.7+}$ and $Pr^{3.9+}$ for samples processed in oxidizing atmosphere, which achieve fluorite-type phases, and $Pr^{3.07+}$ for the C-phase of the eutectic processed in 5%H_2(Ar) (Pr ions are assumed to be fully reduced in A-like phases). Translating these oxidation states to oxygen stoichiometry, allowing for the cation composition of each phase, we find that the number of oxygen vacancies pfu varies between 0.06 and 0.13 in the fluorite phases of samples processed in air or O_2 and ∼0.35 in the C-phase of the eutectic processed in 5%H_2(Ar). These values agree with the assumption that for high enough vacancy concentration (typically 0.25 pfu), the fluorite lattice is no longer stable so that, in the absence of cation ordering, an evolution to a vacancy-ordered C-like phase takes place. Interestingly, the vacancy concentration determined for the low-Pr phase of the eutectic processed in 5%H_2(Ar) is just in the range of the C-phase stability at high temperature according to Rouanet's PD. Because of the fast cooling involved in LFZ, the high-temperature C phase is preserved metastably at RT instead of segregating into pyrochlore + A-phase. In contrast, in oxidizing atmospheres, this high-temperature C-phase evolves to a fluorite phase upon oxidation during cooling.

The particular behavior of the sample processed in O_2 can be understood as follows: Just after crystallization, even in O_2 atmosphere, a C + A eutectic with highly reduced Pr ions is expected to develop. As the temperature decreases, both phases become increasingly oxidized. The low-Pr C-phase can easily accommodate Pr^{4+} ions and oxygen excess, eventually transforming to a fluorite phase, but the high-Pr A-phase cannot stand neither the reduced size of Pr^{4+} nor the higher O content. We may now recall that in the $PrO_{1.5+\delta}$ system, different stable and/or metastable phases form depending on the oxygen partial pressure and thermal history.[28,29] At the high temperatures where phase evolution takes place in LFZ-processed samples (≫1000°C), the stable phases are as follows: A-Pr_2O_3, in highly reducing conditions; a C-like $PrO_{1.5+\delta}$ phase, for moderate oxygen excess, and a defective fluorite PrO_{2-z} phase for high oxygen content (θ, σ, and α phases in Eyring's notation, respectively). Interestingly, the transition from A to C-like phases as the oxygen content increases seems to occur through a phase separation region of A + C type above 900°C.[28]

Transferring these ideas to the high-Pr phase of the eutectic, we propose that in O_2 phase, segregation occurs *within the A–phase lamellae* into a Pr-rich reduced A-like phase at the center and a Pr-poor oxidized C-like region (which oxidizes to fluorite on cooling) toward the interfaces with the low-Pr phase, resulting in a narrowing of the Pr rich lamellae, as observed. Although the appearance is still that of a lamellar eutectic, it should be considered more an intermediate between the initial (partially reduced) state, with eutectic microstructure, and the final (fully oxidized) state, consisting probably of a single, defective fluorite phase. The decrease of the compositional separation between Pr-rich and Pr-poor phases (Δ) as the atmosphere becomes more oxidizing supports our hypothesis. With this interpretation, the ZrO_2–PrO_x system would behave the same as the related ZrO_2–CeO_x system, where a eutectic point exists in the fully reduced ZrO_2–Ce_2O_3 system,[11] but not in the oxidized ZrO_2–CeO_2 case.[12]

At this point, we note that both XRD and Raman results of the present work support the assignment of the low Pr phase in neutral or reducing atmosphere to a C-like phase. We have found no evidence of the "tetragonally-distorted fluorite" phase proposed in Ref. [6].

More interesting is the finding in air atmosphere of a eutectic with two fluorite phases of close composition. Michel et al.[8] studied the growth relations between the phases of ZrO_2–R_2O_3 eutectics (R = Nd, Sm, Dy) produced by the skull-melting technique in air and found two C-type phases with close lattice parameters for R = Dy. The relative crystallographic orientation is termed *syntaxy*, that is, the intergrowth of both phases with the parallelism of equivalent planes and directions. For the mixed-valence Pr case, we have proposed that in oxidizing atmosphere both C phases evolve toward fluorite phases. Although the syntaxy conformation may occur, we speculate that there may

be a different local ordering at the microscopic level in both fluorite phases, reminiscent of the initially reduced state, but elucidating this point is out of the scope of this work.

Our results imply a difference between LFZ-processed samples and those quenched from the melt in air,[7] as regards the symmetry of the high-Pr phase in oxidizing atmosphere. Although LFZ involves fast cooling, it is not as fast as a quenching, and oxygen uptake can occur during cooling, resulting in two fluorite phases instead of the C + A combination found in samples quenched from the melt in air.[7]

A considerable difference is expected also between samples produced by LFZ and those synthesized by low-temperature techniques, such as sol–gel processing methods[2] or coprecitipitation.[5] In LFZ-processed samples, Pr is highly reduced in any atmosphere at high temperature, and the final oxidation state will depend on the kinetics of oxygen diffusion relative to cooling rate. For fast cooling rates, the obtained phases may not be those predicted by the PD in equilibrium and closer to the high temperature ones. In samples produced at low temperatures, on the other hand, size effects *metastabilise* high symmetry phases, and the final structures and oxidation states will depend both on cation and anion diffusivities, probably leading also to nonequilibrium phases. This may explain, for instance, why only F-like phases are obtained in Ref. [2] for 1:3, 1:1, and 3:1 Zr:Pr ratios after calcining at 900°C in air. It may also explain why the F-like $Pr_{0.98}Zr_{0.02}O_x$ compound, previously annealed in air at 900°C, transforms to a C-phase after a reducing treatment at 900°C in Ref. [5], instead of to the expected A-like phase.

We may also comment on the composition of the A-like phases obtained in neutral or reducing atmosphere. EDX analyses evidence a low but non-negligible 12%–13%ZrO_2 content in those phases, which is larger than the ~3%ZrO_2 solubility predicted by the equilibrium PD. The anomaly may arise from two sources: First, the fast cooling involved in LFZ processing may yield at RT a metastable phase with much higher Zr content, similar to the one forming the eutectic at the crystallization temperature. Second, it might occur that the Zr content is overestimated in EDX analyses because of the narrow width (<1 μm) of the light-contrast phases. In fact, the cell volumes obtained for the A-like phases from XRD data (77.3–77.4 Å^3) are marginally lower than that of A-Pr_2O_3 ($V_f \approx 77.5$ Å^3).[30] The Raman shifts of the modes attributable to the high-Pr phase are also very close to those of Pr_2O_3, which suggests a low Zr content.[19]

As regards the potential applicability of these mixed oxides, the more homogeneous, almost single-phase composites obtained in oxidizing conditions are likely to provide better catalytic properties. Composites obtained under neutral or reducing conditions, where one of the phases is of the A-R_2O_3 type, are not expected to present the high oxygen conductivity required for fast redox processes to take place, because of their low tolerance to oxygen stoichiometry variations.

5 | SUMMARY AND CONCLUSIONS

We have processed by the laser-assisted directional solidification technique eutectic composites of the ZrO_2–PrO_x system in O_2, air, N_2, and 5%H_2(Ar) atmospheres. The composition and symmetry changes found in the different atmospheres are compared with results from the literature for the same or related systems, notably ZrO_2–R_2O_3 eutectics or single-phase compounds.

The phase content is C + A in neutral or reducing atmosphere, but two fluorites of close composition are found in air atmosphere with the present processing technique, which implies fast cooling rates. Our results suggest that in the limit of total oxidation, no eutectic would form, in analogy with the ZrO_2–CeO_2 case. The present results agree with previously reported ones in reducing atmosphere but provide evidence of different crystallochemistry in oxidizing atmosphere. Both C- and A-like phases formed under reducing atmosphere at high temperature transform to F-type upon exposure to an oxygen-rich environment.

Differences between LFZ-processed samples and quenched ones are highlighted and attributed to the different cooling rates inherent to both techniques. Cooling kinetics is as important as pO_2 in establishing the final oxidation degree and phase symmetry. Composites processed in highly oxidizing conditions are likely to perform better as catalyst materials. Our work also evidences the relevance of the synthesis method and of the initial state of the sample previous to any thermal treatment.

ACKNOWLEDGMENTS

The authors acknowledge financial support from the Spanish Government through grants PID2019-107106RB-C32, PID2021-124863OB-I00, and BES-2017-079683, funded by MCIN/AEI/10.13039/501100011033 and the European Union through "ERDF A way of making Europe." The Gobierno de Aragón is acknowledged for the financial support to the research group T02-20R. We thank the Servicio General de Apoyo a la Investigación (Universidad de Zaragoza) for technical support in X-ray diffraction, magnetic susceptibility and electron microscopy experiments.

ORCID

María Luisa Sanjuán https://orcid.org/0000-0002-5793-2058

REFERENCES

1. Putna ES, Vohs JM, Gorte RJ, Graham GW. An examination of praseodymia as an oxygen-storage component in three-way catalysts. Catal Lett. 1998;54:17–21.
2. Narula CK, Haack LP, Chun W, Jen H-W, Graham GW. Single-phase PrO_y-ZrO_2 materials and their oxygen storage capacity: a comparison with single-phase CeO_2-ZrO_2, PrO_y-CeO_2, and PrO_y-CeO_2-ZrO_2 materials. J Phys Chem B. 1999;103:3634–9.
3. Logan AD, Shelef M. Oxygen availability in mixed cerium/praseodymium oxides and the effect of noble metals. J Mater Res. 1994;9:468–75.
4. Yu Sinev M, Graham GW, Haack LP, Shelef M. Kinetic and structural studies of oxygen availability of the mixed oxides $Pr_{1-x}M_xO_y$ (M = Ce, Zr). J Mater Res. 1996;11:1960–71.
5. Abel J, Lamirand-Majimel M, Majimel J, Bellière-Baca V, Harlé V, André G, et al. Oxygen non-stoichiometry phenomena in $Pr_{1-x}Zr_xO_{2-y}$ compounds ($0.02 < x < 0.5$). Dalton Trans. 2014;43:15183–91.
6. Krasil'nikov MD, Vinokurov IV, Nikitina SD. Physicochemical properties of solid solutions in the zirconium dioxide–praseodymium oxide system in air; in Fiz. Khim. Elektrokhim. Rasplavl. Tverd. Elektrolitov, Tezisy Dokl. Vses. Konf. Fiz. Khim. Ionnykh Rasplavov Tverd. Elektrolitov, 7th, Sverdlovsk, USSR, September 18–20, 1979, Vol. 3, pp. 123–125. Akademiya Nauk SSSR, Ural'skii Nauchnyi Tsentr, Ekaterinburg, USSR. 1979.
7. Rouanet A. Contribution a l'étude des systèmes zirconia—oxydes des lanthanides au voisinage de la fusion: mémoire de thèse. Rev Intern Hautes Temper Refract. 1971;8:161–80.
8. Michel D, Rouaux Y, Perez y Jorba M. Ceramic eutectics in the systems ZrO_2-Ln_2O_3 (Ln = Lanthanide): unidirectional solidification, microstructural and crystallographic characterization. J Mater Sci. 1980;15:61–6.
9. Andrievskaya ER. Phase equilibria in the refractory oxide systems of zirconia, hafnia and yttria with rare-earth oxides. J Eur Ceram Soc. 2008;28:2363–88.
10. Aldebert P, Traverse JP. Étude par diffraction neutronique des structures de haute témperature de La_2O_3 et Nd_2O_3. Mat Res Bull. 1979;14:303–23.
11. Negas T, Roth RS, McDaniel CL, Parker HS, Olson CD. Influence of K_2O on the cerium oxide-ZrO_2 system. In: Lundin CE, editor. Proceedings of the 12th rare earth research conference. Vol. II. Vail, Colorado, USA: University of Denver; 1976. p. 605–14.
12. Yashima M, Morimoto K, Ishizawa N, Yoshimura M. Diffusionless tetragonal–cubic transformation temperature in zirconia–ceria solid solutions. J Am Ceram Soc. 1993;76:2865–8.
13. Rodriguez-Carvajal J. FULLPROF: a program for Rietveld refinement and pattern matching analysis, abstracts of the satellite meeting on powder diffraction of the XV Congress of the IUCr, p. 127. Toulouse, France; 1990.
14. Llorca J, Orera VM. Directionally solidified eutectic ceramic oxides. Prog Mater Sci. 2006;51:711–809.
15. Heremans C, Wuensch BJ, Stalick JK, Prince E. Fast-ion conducting $Y_2(Zr_yTi_{1-y})_2O_7$ pyrochlores: neutron Rietveld analysis of disorder induced by Zr substitution. J Solid State Chem. 1995;117:108–21.
16. Adachi G-y, Imanaka N. The binary rare earth oxides. Chem Rev. 1998;98:1479–514.
17. Shannon RD. Revised effective ionic radii and systematic studies of interatomic distances in halides and chalcogenides. Acta Crystallogr, Sect A. 1976;A32:751–67.
18. Sanjuán ML. Raman spectroscopy study of disorder phenomena and size effects in pyrochlores. In: Chowdhury A, editor. Pyrochlore ceramics: properties, processing, and applications. Elsevier series on advanced ceramic materials. Amsterdam: Elsevier; 2022. p. 95–159.
19. Zarembowitch J, Gouteron J, Lejus AM. Raman spectra of lanthanide sesquioxide single crystals with A-type structure. Phys Status Solidi B. 1979;94:249.
20. Swanson BI, Machell C, Beall GW, Milligan WO. Vibrational-spectra and assignments for lanthanide trihydroxides. J Inorg Nucl Chem. 1978;40:694–6.
21. Sanivarapu SR, Lawrence JB, Sreedhar G. Role of surface oxygen vacancies and lanthanide contraction phenomenon of $Ln(OH)_3$ (Ln = La, Pr, and Nd) in sulfide-mediated photoelectrochemical water splitting. ACS Omega. 2018;3:6267–78.
22. Orera A, Larraz G, Sanjuán ML. Spectroscopic study of the competition between dehydration and carbonation effects in La_2O_3-based materials. J Eur Ceram Soc. 2013;33:2103–10.
23. Ubaldini A, Carnasciali MM. Raman characterisation of powder of cubic RE_2O_3 (RE = Nd, Gd, Dy, Tm, and Lu), Sc_2O_3 and Y_2O_3. J Alloys Compd. 2008;454:374–8.
24. Phillippi CM, Mazdiyasni KS. Infrared and Raman spectra of zirconia polymorphs. J Am Ceram Soc. 1971;54:254.
25. Dogra S, Singh J, Sharma ND, Samanta K, Poswal HK, Sharma SM, et al. Phase progression via phonon modes in lanthanide dioxides under pressure. Vib Spectrosc. 2014;70:193–9.
26. Kern S. Magnetic susceptibility of praseodymium oxides. J Chem Phys. 1964;40:208–12.
27. Foex M, Traverse J-P. Étude du polymorphisme des sesquioxydes de terres rares à haute température. Bull Soc franç Minér Crist. 1966;89:184–205.
28. Hyde BG, Bevan DJM, Eyring L. On the praseodymium + oxygen system. Philos Trans R Soc London, Ser A. 1966;259:583–614.
29. Burnham DA, Eyring L. Phase transformations in the praseodymium oxide-oxygen system: high-temperature X-ray diffraction studies. J Phys Chem. 1968;72:4415–24.
30. Greis O, Ziel R, Breidenstein B, Haase A, Petzel T. The crystal structure of the low-temperature A-type modification of Pr_2O_3 from X-ray powder and electron single crystal diffraction. J Alloys Compd. 1994;216:255–8.

SUPPORTING INFORMATION

Additional supporting information can be found online in the Supporting Information section at the end of this article.

How to cite this article: Grima L, Peña JI, Sanjuán ML. Ceramics with eutectic microstructure in the ZrO_2–PrO_x system. J Am Ceram Soc. 2023;1–11. https://doi.org/10.1111/jace.19305